Wave-number selection and parity-breaking bifurcation in directional viscous fingering

Ludovic Bellon,* Laurent Fourtune, Vahé Ter Minassian, and Marc Rabaud†
Laboratoire de Physique Statistique de l'Ecole Normale Supérieure, associé au CNRS et aux Universités Paris VI et VII, 24 rue Lhomond, 75231 Paris Cedex 05, France
(Received 30 December 1997)

We present a mechanism of limitation for the possible wave numbers above an instability threshold. This mechanism is experimentally investigated in the interfacial instability of directional viscous fingering in a finite system. It is shown experimentally to be controlled by the divergence of a phase-diffusion constant. Theoretically, this limitation on the low value of the accessible wave numbers is a consequence of the interaction between the fundamental and the first harmonic modes. The analysis of coupled amplitude equations demonstrates theoretically the existence of a divergence of a phase-diffusion constant when approaching the threshold of a parity-breaking instability. [S1063-651X(98)13307-X]

PACS number(s): 47.20.Hw, 47.54.+r, 47.20.Ky, 47.20.Ma

I. INTRODUCTION

The nonlinear mechanism that limits the range of the unstable modes above threshold in a spatially extended dissipative system has been a puzzling subject for many years [1]. This problem had been investigated experimentally, numerically, and theoretically in particular in model systems such as Taylor-Couette flow [2], Rayleigh-Bénard convection [3], and in interfacial instabilities such as directional solidification [4], Taylor-Dean flow [5], directional viscous fingering [6], and Rayleigh-Taylor instability [7]. Usually the selection is well understood close to onset, but not in the nonlinear regime. A first general selection mechanism for a one-dimensional system is the Eckhaus instability [8]. Other mechanisms specific to the convection case were investigated by Busse [9] and the effect of the boundaries were investigated more recently [2,10].

We present here a study of a mechanism encountered in the directional viscous fingering instability. It is found to be closely related to the parity-breaking bifurcation of an interface, a secondary instability that was described by Coullet, Goldstein, and Gunaratne [11], Fauve, Douady, and Thual [12], and Caroli, Caroli, and Fauve [13]. Some preliminary results of this study were presented in Ref. [14].

This paper is organized as follows. In Sec. II we present the experimental results: the setup (II A), the stable states (II B), the processes of nucleation or death of a cell (II C). Then we present the phase-dynamic behavior and the evolution of the phase-diffusion coefficient (II D) and we conclude this experimental part with a description of a long-lived self-oscillating transient (II E). In Sec. III we interpret the results within the framework of the ''k-$2k$'' model (III A) and of an ''antisymmetry'' model (III B).

II. EXPERIMENTAL RESULTS

A. Experimental setup

Our experimental setup is an enlarged version of the one presented in Refs. [14] and [15]. A floated glass plate (plane at $\pm 10\ \mu$m over 50 cm) is lying horizontally over a steel rectified cylinder of radius $R = 50 \pm 0.01$ mm and length 420 mm (Fig. 1). The cylinder is partially immersed in an oil tank thermostatically controlled at 32 ± 0.1 °C. Rotation extrudes from the tank a film of oil. This film fills the small gap between the cylinder and the plate, and the excess oil flows back down along the cylinder. The amount of oil passing through the nip is controlled by the minimum distance b_0 between the plate and the cylinder. At low velocity the downstream meniscus is located at a constant distant from the nip. When observed from above through the glass plate, it appears as a line parallel to the cylinder axis. When the cylinder speed is increased, this meniscus becomes unstable [6]. Our setup is similar to those found in the coating industry, where the instability is known as the ribbing instability [16]. At threshold, the downstream meniscus undergoes a supercritical bifurcation to a stationary sinusoidal state of

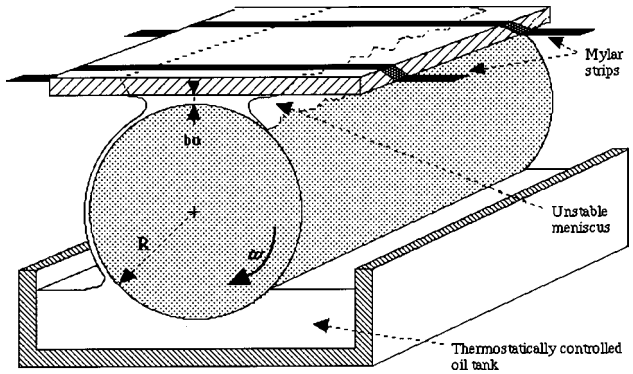

FIG. 1. Scheme of the experimental setup. The rotating cylinder extrudes the oil from a thermostated bath. This oil fills the upper nip between the cylinder and the horizontal glass plate. The downstream meniscus is unstable if the rotation is fast enough. Two plastic strips are located in the nip and serve as boundaries for the interface. The displacement of one of the strips is controlled by a computer and a stepper motor.

*Present address: Laboratoire de Physique de l'Ecole Normale Supérieure de Lyon, 46 Allée d'Italie, 69364 Lyon Cedex 07, France.

†Present address: Laboratoire FAST, associé au CNRS et aux Universités Paris VI et XI (UMR 7608), Bâtiment 502, Campus Universitaire, 91405 Orsay Cedex, France. Electronic address: rabaud@fast.u-psud.fr

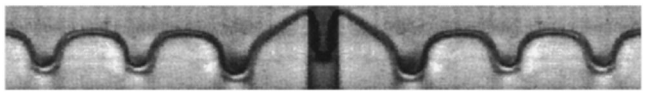

FIG. 2. Image of the downstream meniscus above threshold. The dark line separates the air (below) from the oil (above). In the central portion, the plastic strip is visible as it deforms the pattern, which is otherwise regular and static. On each side of the strip, the first oil rib is fixed in position. Thus the strip acts as a rigid boundary condition for the phase of the pattern.

uniform finite wavelength. This transition is characterized by a critical value Ca* of the capillary number $\mathrm{Ca}=\mu V/T$ [17]. This critical value depends on the thickness b_0. In the present study the thickness is kept constant ($b_0=0.4$ mm) and we used a silicon oil (Rhodorsyl V20) of surface tension $T=20.9\times10^{-3}$ N/m and viscosity $\mu=0.020$ kg/m s. The critical tangential velocity is thus 220 mm/s, which corresponds to $\mathrm{Ca}^*\approx0.20$. The rotation of the cylinder is controlled by a DC motor with a velocity resolution of ±1 mm/s. The interface is observed from above by a charge-coupled-device (CCD) camera. The video signal is digitized on a computer and can be analyzed with the freeware NIH Image.

In this particular setup, as in Ref. [14] and in contrast with previous experiments [18,19], we can impose the length L of the interface by positioning two plastic strips that fill almost completely the gap between the glass and the cylinder (Fig. 1). The maximum value of L that we can use is 20 cm due to the limited flatness of the float glass on larger scales. The plastic strips are mounted on carriages that can run along the cylinder axis. One of the two carriages is controlled by a stepper motor and an endless screw, allowing one to set the position of the strip with a relative precision of 10 μm. Each strip acts as a boundary for the interface, and fixes the neighboring cell at a constant distance from the strip (Fig. 2). Thus we can introduce an effective length of the box L^* defined as the real size L minus the width of the two trapped cells. In contrast with the case of low thickness gradient [19], here the interface does not present very deep air fingers, but smooth cells above threshold.

B. Permanent stable states

1. Stable wave numbers

Increasing or decreasing the velocity V, we observe changes of wave number. However, after some transients the interface always evolves to a static periodic shape of constant wave number k in the domain L^*. These stable states are only observed in a domain of the (Ca,k) plane: for any velocity, depending on the history, any value of k in this domain can be obtained (Fig. 3). In order to observe the limits of the wavelength range of the pattern, a first set of experiments at fixed size L were realized. Increasing the velocity V (and therefore Ca) by small steps of 1%, we measure the wave number of the last observed stable pattern, preceding the nucleation of a new cell. These data give one limit of the wave-number range. The other limit can be determined the same way by decreasing the velocity and watching for disappearance of cells. Figure 3 illustrates the stable states we have observed for an average size of the

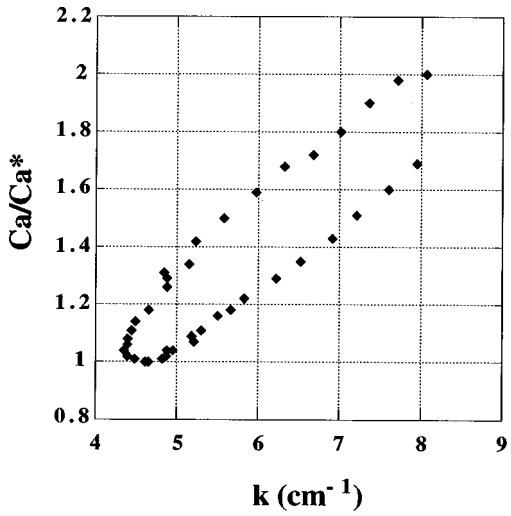

FIG. 3. Limits of observed stable wave numbers k versus the normalized control parameter Ca/Ca*. Observed steady states lie in the central tongue. The plotted data represent the last observed permanent state before a nucleation or a disappearance of a cell. The plot is a compilation of the results obtained by increasing or decreasing quasistatically either the velocity or the length of the interface around a mean value $L=20$ cm.

interface $L=20$ cm. No meaningful change in this diagram was noticed for the different values of L we have explored ($L\geqslant6$ cm). This shows that finite-size effects are not important when the number of cells is larger than a few units (5 or 10). At low wave numbers, we completed the diagram by varying L around its average value (variations of about 10%): ''Horizontal'' runs (for a given Ca/Ca*) were more suited to this region. Increasing L by small steps, k decreases and we can measure the wave number before nucleation and this gives the left boundary of the wave-number range, whereas decreasing L leads to the disappearance of one cell, limiting the wave-number range on the right-hand side (Fig. 3). After any step in L or Ca, we waited at least 5 min to check the pattern stability. A similar technique of varying L was used by Ahlers *et al.* [2] for their study of the stability of the wave number in Taylor vortex flow.

Figure 3 shows that a wave number is stable in a finite range of capillary number. These results are in clear contrast with the observed evolution of the wave number in the same experiment when no plastic strips were present [19]. In that case, where the lateral boundary conditions for the phase were ''free,'' we observed a continuous evolution of the wave number with the capillary number, without measurable hysteresis (see Fig. 3 of Ref. [19]).

2. Shape of the interface

Just above the onset of the instability, the interface is sinusoidal and thus exhibits an up/down symmetry [Fig. 4(a)]. When $\mathrm{Ca}/\mathrm{Ca}^*>1.10$, the pattern loses this air-oil symmetry. Air cells become larger and oil domains narrower [Fig. 4(b)]: the harmonics of the fundamental mode have nonzero amplitudes, which gives to the pattern its nonlinear shape.

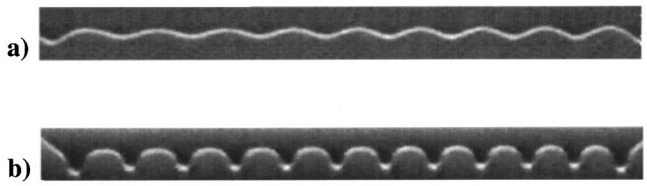

FIG. 4. Images of all the unstable interface ($L \approx 12$ cm) between oil (top) and air (bottom). (a) Symmetric case near onset (Ca/Ca* = 1.04). (b) Nonlinear shape for Ca/Ca* = 1.63 when the air-oil symmetry is broken.

C. Transient states

We will now describe the transients that give rise to an adjustment of the wave number in the vicinity of the limits of Fig. 3.

1. Large wave-number process

When studying the limits of stability in the right-hand limit of Fig. 3, we observe transients that are different from those observed with open boundary conditions [19]. Here, with the rigid boundary conditions, the transient linked to the disappearance of a cell basically follows the same process for all explored Ca. As illustrated in Fig. 5, one air cell slowly starts shrinking and loses amplitude, then disappears suddenly. The two neighbors form for a while a pair of asymmetric air cells. These larger cells shrink while the phase defect diffuses through the whole pattern, leaving a stable pattern with a new wave number $k' = k - 2\pi/L^*$. The whole process is slow, of the order of 30 s in Fig. 5.

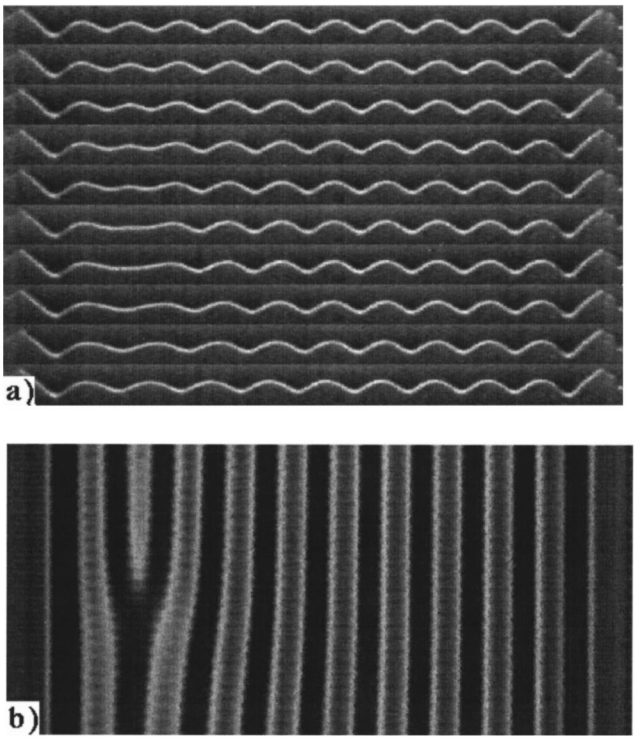

FIG. 5. Evolution of the entire interface during the disappearance of a cell for Ca/Ca* = 1.11. (a) Ten successive snapshots showing the death of the second air cell from the left. Time progresses 30 s from top to bottom but there is no constant delay between each image. (b) Temporal evolution of one horizontal video line crossing the interface during the same event and for the same duration. Oil domains appear darker than air domains. Again and as in all the figures, time progresses from top to bottom.

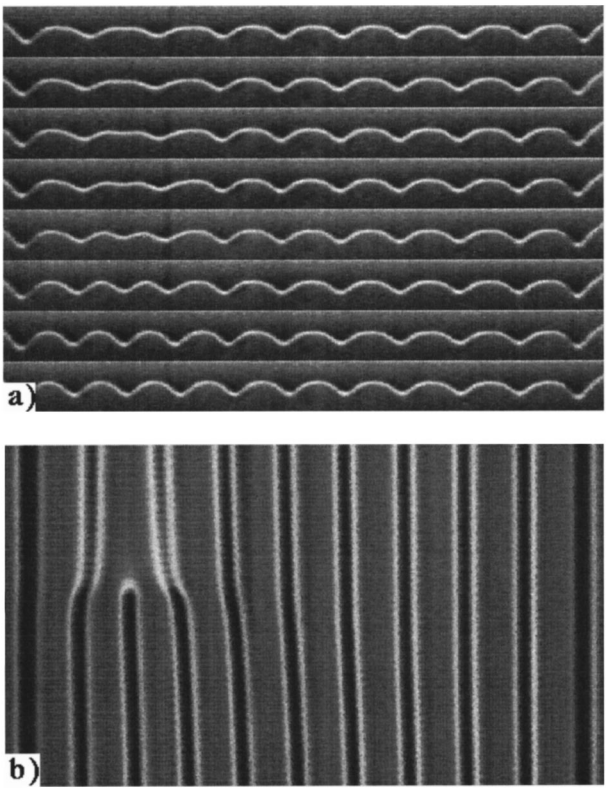

FIG. 6. Evolution of the entire interface during a nucleation for Ca/Ca* = 1.26. (a) Eight successive snapshots. Time progresses 40 s from top to bottom with nonconstant delay between each image. (b) Temporal evolution of one horizontal video line during the same event and for the same duration.

2. Low wave-number process

Contrary to the preceding case, the nucleation process observed in the left-hand limit of Fig. 3 depends on the value of Ca. The transients are different for small or large Ca.

For small values of the capillary number (Ca/Ca* < 1.32), one air cell slowly starts increasing its length and losing amplitude (Fig. 6). The process that concentrates this phase defect is fairly long. Then, an oil indentation quickly grows at the tip of this air cell and the two new cells grow while the phase defect diffuses through the whole pattern. Conversely, as can be seen in Fig. 7 for larger Ca (Ca/Ca* > 1.32), the transient begins suddenly when one oil domain changes shape; the two neighboring air cells lose their left-right symmetry, creating a pair of abnormal cells [19], the amplitudes of which are smaller whereas their lengths are larger. These abnormal cells have quite a long life (a few seconds). The separating oil domain then starts oscillating from left to right, and finally splits into two different oil domains separated by a new air cell. The nucleation processes are thus quite different according to the value of Ca: for weak Ca, one oil domain grows in an air cell, whereas for strong Ca, one air cell grows in an oil domain.

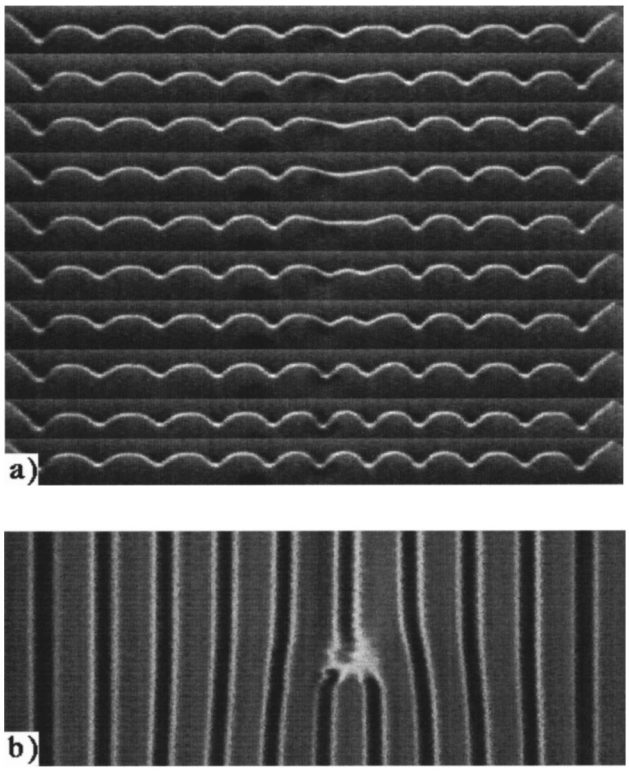

FIG. 7. Evolution of the entire interface during a nucleation for $Ca/Ca^* = 1.34$. (a) Ten successive snapshots. Time progresses 50 s top to bottom in with nonconstant delay between each image. (b) Temporal evolution of one horizontal video line during the same duration.

We will see in the next paragraph that these two different processes for nucleation can be linked to the response of the pattern to small perturbations.

D. Measurement of the phase-diffusion coefficient

1. Demonstration of a diffusive process for the phase of the pattern

Following the works of Wesfreid and Croquette [20] and Wu and Andereck [21] and with the aim of characterizing the Eckhaus limit, we tested the response of the pattern to a small perturbation. We introduced an oscillating boundary by imposing a sinusoidal motion to one of the plastic strips. After a transient, the whole pattern oscillates at the forcing frequency f, but the perturbation is attenuated and out of phase far away from the oscillating wall (Fig. 8). The attenuation from cell to cell of the amplitude of oscillation is well fitted by an exponential curve with a decreasing factor α, whereas the phase of the oscillation appears to have a linear behavior of slope β. The phase of the perturbation can therefore be written $\varphi(x,t) = \varphi_0 \exp[-(\alpha + i\beta)x + i\omega t]$, where x is the distance to the oscillating side [21]. The two coefficients α and β can be determined from the spatiotemporal image of Fig. 8.

We have checked experimentally that for a wide range of frequencies f, $\alpha \approx \beta$ and that the two coefficients scale as $f^{1/2}$ (Fig. 9). These results are typical of a diffusion equation for the phase of the pattern: $\varphi_t = D\varphi_{xx}$. The diffusion coefficient D is then given by $D = \pi f/\alpha\beta$ [21].

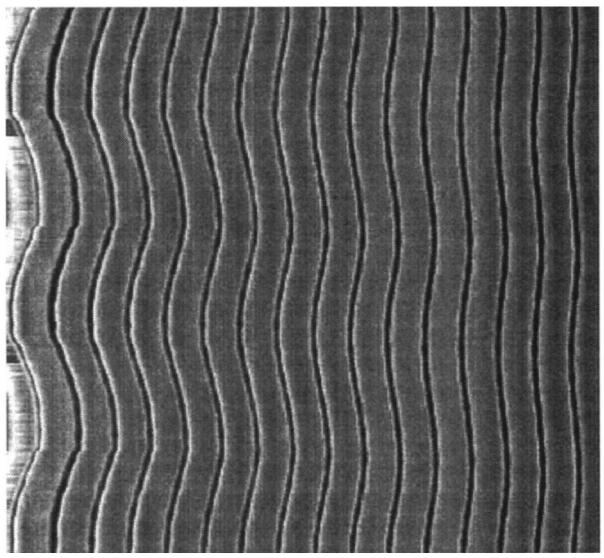

FIG. 8. Forced oscillations of the pattern. This picture shows the evolution of one video line cutting the interface. Time progresses 530 s from top to bottom. The plastic strip (left) oscillates with a frequency $f = 0.005$ Hz. The amplitude oscillation is very large in order to obtain an easily observable deformation. The perturbation of the oil ribs (dark) is attenuated and the phase shift from rib to rib increases linearly with the distance from the plastic strip.

2. Experimental procedure

For various capillary numbers, we want to measure the diffusion constant D varying the wave number k, which can be tuned by changing the size of the box. We must then choose the average length L of the interface, the amplitude A, and the frequency f of the oscillation. These three parameters must satisfy contradictory needs. Length L must be large enough to have a large number of cells but not too

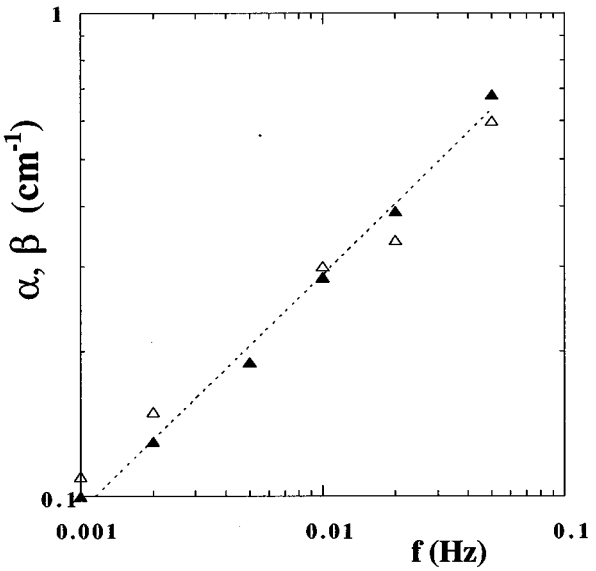

FIG. 9. Evolution of α and β vs the frequency f of the oscillation on log-log scales. Within the limits of the precision of the measurements, $\alpha = \beta$. The dashed line represents the best power-law fit, whose slope is 0.48.

large, because the diffusion time scales as L^2 and transients become too long. The amplitude A of the perturbation has to be large enough to be measured (a few pixels wide) but not too large compared to the wavelength, especially when reaching the borders of the stable domain where the interface becomes very fragile. Finally, the frequency f must be low enough to have a large penetration depth of the oscillation, but not so low as to avoid the reflection of the oscillation on the fixed boundary. We chose to work with an average size $L=10$ cm (which leads to a typical diffusion time along the interface of 500 s), an amplitude of the perturbation $A=0.6$ mm (less than 10% of the wavelength), and a frequency $f=0.02$ Hz. These values allow for good precision in a reasonable amount of time. We explored the values Ca/Ca*$=1.16$, 1.30, 1.50, 1.65, and 1.80.

3. Behavior of the phase-diffusion coefficient versus k

For low capillary number (Ca/Ca*$=1.16$, 1.30), as shown in Fig. 10(a), D is decreasing at the extremities of the wave-number range. The values of D for extreme k are almost half the values of D for a mean k. This result is the classical result observed in other experiments exhibiting an Eckhaus instability [20,21].

For high capillary number (Ca/Ca*$=1.65$ or 1.80), the behavior of D is quite different from the previous one: if a decrease of D for the largest k can still be seen, the trend for the smallest k is opposite [Fig. 10(b)]. A growth of 50–150 % of D when k decreases to its smallest value can be measured for Ca/Ca*$=1.65$. This quick growth of D toward the high values of Ca and low values of k is also illustrated by Fig. 11 which plots the behavior of D with Ca for a given k (the size of the box L and the number of cells is fixed for the whole run). We can see that D is 2 or 3 times larger for the highest Ca than for a mean Ca, whereas it is slowly decreasing for the smallest values of Ca.

For intermediate capillary numbers (Ca/Ca*$=1.50$), the behavior of D corresponds to a blend of the two previous behaviors (Fig. 12). If the decrease for the largest k is still observed, the behavior on the other edge of the wavelength range is less clear. We were unable to determine whether the transition between the decreasing and growing behaviors is easy through a state where D goes to a finite nonzero value or if it is a fairly sharp jump from zero to $+\infty$ [22].

The behavior of D for small Ca is close to the theoretical behavior of the Eckhaus instability: the decreasing of D to 0 on the edges of the wave-number range is the signature of such an instability [8]. Experimentally, it is not possible to reach these very low values of D because any finite-amplitude perturbation induces a change of wave number. The behavior of D for larger Ca can be interpreted the same way for the largest k: its decrease on the right-hand side of the wavelength range is clear but not strongly marked because here also it is experimentally difficult to perturb the extreme values of k. The unexpected result is the quick growth of D for the smallest k, but as we will show in part III, this growth can be ascribed to the proximity of a parity-breaking bifurcation.

E. Self-oscillating states

When we abruptly increase Ca, we sometimes observe a long transient self-oscillating state of the pattern (Fig. 13). In this state, all the cells shift in phase alternately to the right and to the left. This state usually lasts more than one hour although in all cases when we waited long enough it eventually decayed and disappeared [Fig. 13(a)], which makes it a transient. This transient state is characterized by extremely low oscillation frequencies ($T \geqslant 100$ s). Similarly, slow oscillations have been observed in a Taylor-Couette system [23]. The oscillation amplitude of each cell varies according to its position along the interface. This amplitude is well fitted by a sine function and thus corresponds to the first resonant mode of the effective interval L^* (Fig. 14). For fixed values of the parameters, we also measure the period of the oscillations as a function of the size L^* of the box. This is difficult to realize, as we are not able to trigger these transients. However, the evolution of the frequency of oscil-

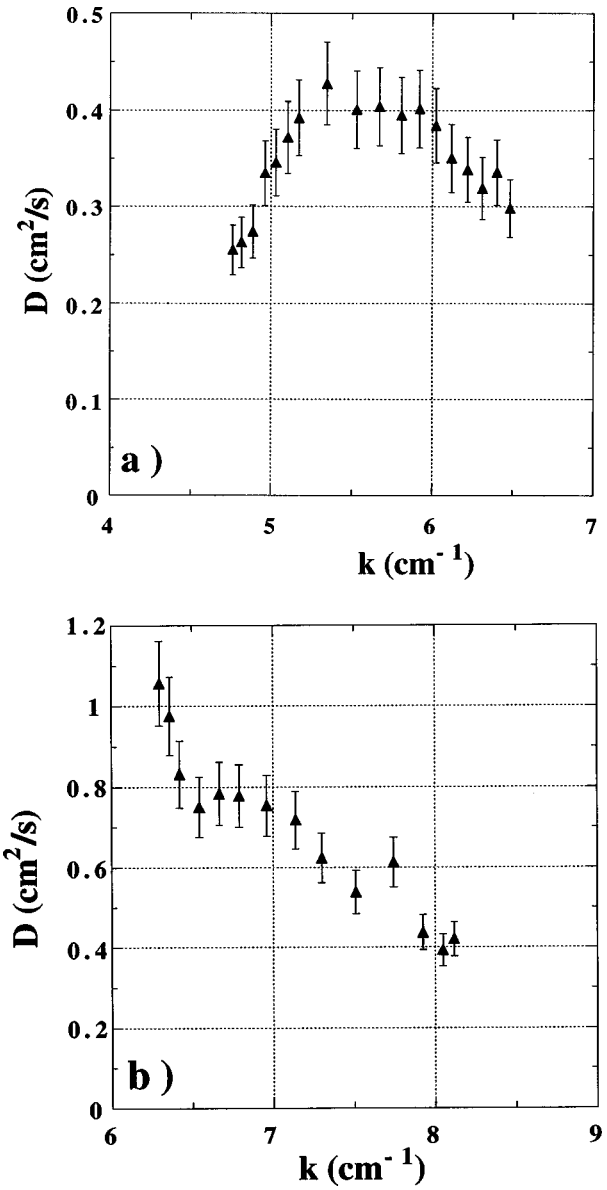

FIG. 10. Evolution of D vs k for $L=10$ cm and for two values of Ca. Error bars show the extreme measured values. (a) Ca/Ca*$=1.30$. D decreases on both edges of the wave-number range, which characterizes an Eckhaus instability process. (b) Ca/Ca*$=1.65$. D decreases for large k, whereas it increases for small k.

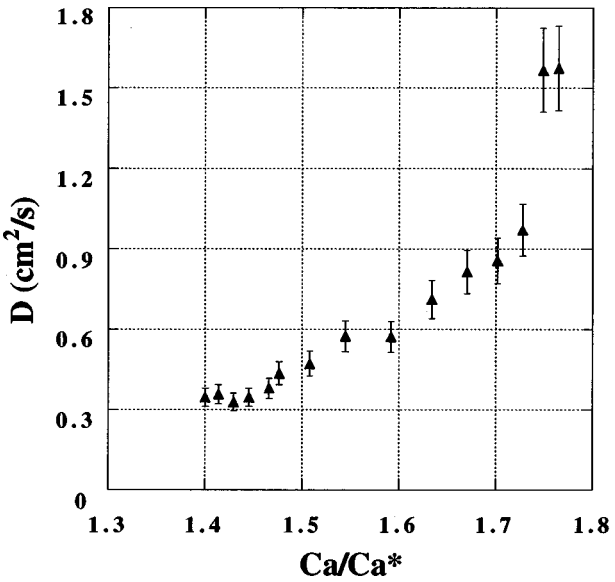

FIG. 11. Evolution of D vs Ca for $k=6.8\,\mathrm{cm}^{-1}$ and $L=10$ cm. The coefficient D decreases for small Ca and increases for large Ca.

lations with L^* is compatible with a linear behavior (Fig. 15). Most of these results may be understood through the model coupling phase and antisymmetry presented in Sec. III C.

III. THEORETICAL INTERPRETATION

A. Long-wavelength instability of the k-$2k$ model

There are different ways to model a parity-breaking bifurcation. One of these has been much studied in recent years [12,18,24–26]. It involves the interaction between the first mode k to appear in an instability and its $2k$ harmonic. The presence of this harmonic breaks the air-oil symmetry of the interface [Fig. 4(b)]. The so-called k-$2k$ model can be written as a set of two coupled Ginzburg-Landau equations:

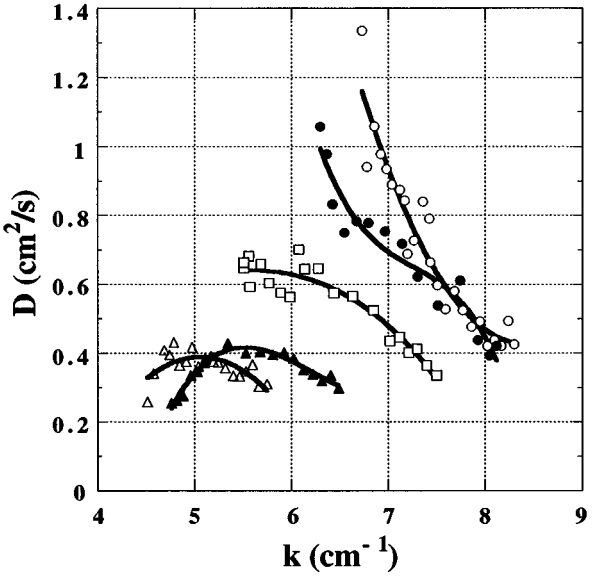

FIG. 12. Behavior of D with k for various values of Ca [Ca/Ca*$=1.16$ (△), 1.3 (▲), 1.5 (□), 1.65 (●) and 1.8 (○)]. The lines are guides for the eyes. If the behavior of D for large k is the same for all Ca, it switches from decreasing to increasing for the smallest k when Ca increases.

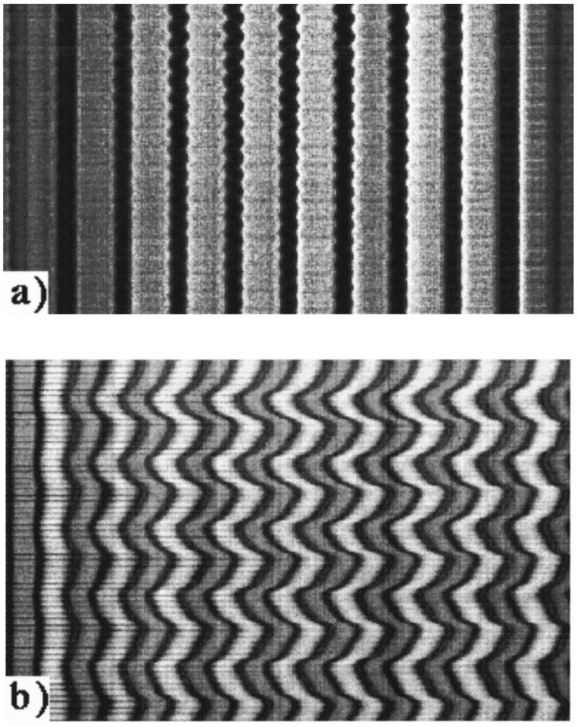

FIG. 13. Spatiotemporal images of self-oscillating states. (a) Ca/Ca*$=1.6$, $L^*=7.1$ cm, and time from top to bottom corresponds to 2500 s. The period is of the order of 130 s. Note that the amplitude of the oscillations decreases slowly with time. (b) Ca/Ca*$=1.2$, $L^*=13.6$ cm, and time from top to bottom corresponds to 2000 s. The period is of the order of 400 s and the amplitude much larger than in case (a). The oscillations are of large amplitude and not sinusoidal. Note that the right-hand boundary is not visible in this picture.

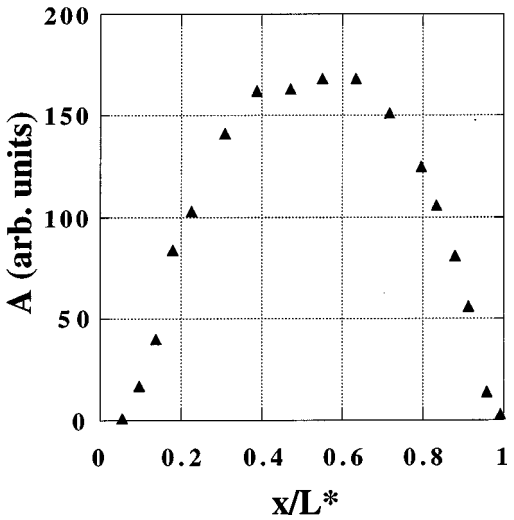

FIG. 14. Amplitude of the oscillation vs the dimensionless abscissa x/L^* corresponding to Fig. 13(b). The dashed line is a fit by a sinusoidal function of period 2.

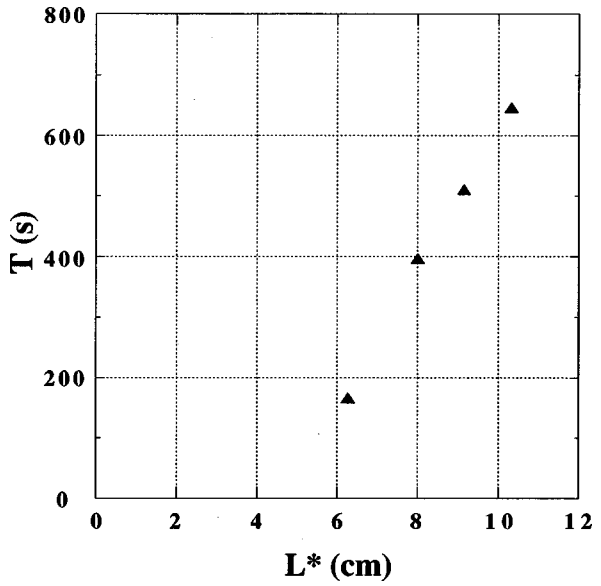

FIG. 15. Period T of the self-oscillation vs the effective size of the cell L^*.

$$\dot{A}_1=\mu_1(k)A_1-\gamma A_1^*A_2-a_1|A_1|^2A_1-b_1|A_2|^2A_1,$$
$$\dot{A}_2=\mu_2(k)A_2+\gamma A_1^2-a_2|A_2|^2A_2-b_2|A_1|^2A_2, \quad (1)$$

with A_1 and A_2 respectively the amplitudes of the first mode and its harmonic. This model is valid in the vicinity of the codimension-2 point, where both μ_1 and μ_2 are small. In our study we will further expand the range of validity of this approximation. The originality of this model lies in the fact that the parity-breaking mechanism is not explicitly introduced in the equations, contrary to other analyses [11]. In fact, the interacting γ terms control the phase shift between modes k and $2k$.

As long as A_2 is strongly damped, the $2k$ mode is slaved to the k mode, and there is no phase shift between them. But when μ_2 gets closer to 0 (but remains negative), the $2k$ mode grows independently and the pattern breaks the right-left parity. This pattern is no longer stationary: all the cells propagate steadily along the interface [26]. This parity-breaking bifurcation occurs on the line where $C=0$, where

$$C=(\mu_1 b-\mu_2 a)^2-\gamma^2(2a+b)(2\mu_1+\mu_2), \quad (2)$$

with $a=2a_1+b_1$ and $b=2a_2+b_2$.

In fact, in experiments, the control parameters μ_1 and μ_2 depend not only on the capillary number Ca but also on the wave number k. Therefore, this parity-breaking bifurcation (PB) condition corresponds to a line in the (Ca,k) plane. In Fig. 16 we plot the two curves ($\mu_1=0$ and $\mu_2=0$) given by the linear stability analysis of the meniscus (Appendix of [18,19]) and we draw the PB line close to $\mu_2=0$ according to previous arguments. Figure 16 shows that the pattern should be stable between the Eckhaus line and the PB line. Beyond the Eckhaus line the pattern is expected to be unstable and to exhibit a behavior consisting of concentration of phase defects, whereas over the PB line, it is likely to exhibit a propagative state or some kind of transient scenario beginning with a parity breaking [4,18,26].

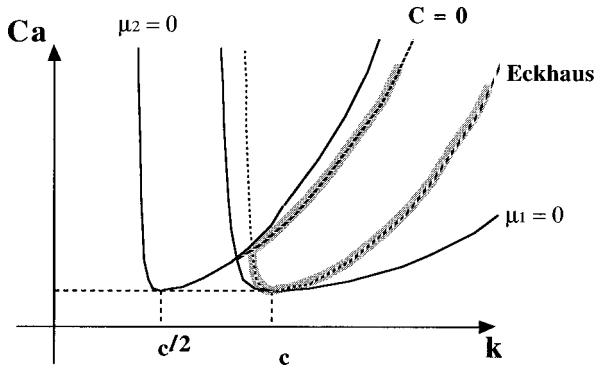

FIG. 16. Theoretical wave-number selection diagram. The line $\mu_1=0$ is the marginal stability of a k mode (appendix of [18,19]), $\mu_2=0$ corresponds to the marginal line for a k mode whose harmonic $2k$ becomes unstable. The $C=0$ line is drawn close to the $2k$ marginal stability curve. The Eckhaus line is deduced from the lower branch by a factor of 3 in (Ca-Ca*)/Ca*. The stable domain is between the Eckhaus and the $C=0$ lines.

However, at this stage, we have not yet proved that the upper limit of the experimental wave number stability range (Fig. 3) is due to a parity-breaking bifurcation. In particular, the large increase of the phase-diffusion coefficient D (Figs. 10–12) has yet to be understood.

Therefore, we study the k-$2k$ coupled equations under infinitely small perturbations q on the wave number k:

$$\begin{aligned}A_1&=A_{1o}[1+a_{1,+q}\exp(st+iqx)\\&\quad+a_{1,-q}\exp(st-iqx)]\exp i(kx+\theta),\\A_2&=A_{2o}[1+a_{2,+q}\exp(st+iqx)\\&\quad+a_{2,-q}\exp(st-iqx)]\exp i(2kx+\varphi),\end{aligned} \quad (3)$$

where the $a_{i,\pm q}$ are small.

We will also expand μ_1 and μ_2 around k to the second order in q:

$$\begin{aligned}\mu_1(k+q)&=\mu_1(k)+q\mu_1'(k)+\frac{q^2}{2}\mu_1''(k)+\cdots,\\\mu_2(k+q)&=\mu_2(k)+q\mu_2'(k)+\frac{q^2}{2}\mu_2''(k)+\cdots.\end{aligned} \quad (4)$$

This leads to a 4×4 matrix on the $a_{i\pm q}$. This matrix has four eigenvalues, three of which are negative. The last one is close to 0 and is given by

$$s=-Dq^2 \quad \text{with} \quad D=\frac{F}{C}, \quad (5)$$

where F is a complicated number which is positive for small enough γ, by continuity with the case $\gamma=0$, and C [defined in Eq. (2)] is positive and goes to zero at the PB bifurcation. Therefore, theory predicts that D will diverge to $+\infty$ in the vicinity of the PB line. This behavior was checked numerically as well (see Fig. 4b of Ref. [14]).

This model first explains why we have observed (II D) this strong increase in D. It also shows that a divergence of D is the *signature* of a parity-breaking bifurcation. We may

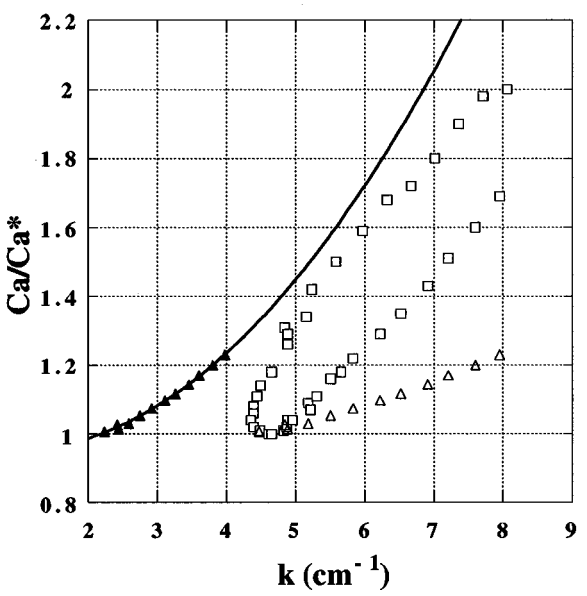

FIG. 17. Experimental wave-number selection diagram. The open squares (□) represent the experimental limits (upper and lower branches) of the observed modes (same as Fig. 3). The open triangles (△) are deduced from the lower branch by a factor of $\frac{1}{3}$ in (Ca-Ca*)/Ca*. Filled triangles are deduced from the open triangles by a horizontal compression factor of 2 in k. The extrapolation of a parabolic fit through these filled triangles (continuous line) is in fair agreement with the upper branch of the experimental data as predicted by the model.

check the validity of this understanding of the wavelength-selection mechanism as a PB bifurcation by deducing the expected position of the PB line on the experimental graph (Fig. 17). In this figure we first plot the experimental data of Fig. 3. From these data, assuming that the lower branch corresponds to the Eckhaus line, we estimate the marginal stability curve ($\mu_1=0$) by a compression by a factor 3 of the Ca axis (this transformation would be exact near threshold for a parabolic marginal stability curve). From this new curve, we deduce the marginal stability curve of the $2k$ mode ($\mu_2=0$) by a compression by a factor 2 of the k axis. The extrapolation of this last curve for large k is close to the experimental low limit of k. The agreement between the two curves is surprisingly good considering the approximated $\frac{1}{3}$ factor between the Eckhaus line and the $\mu_1=0$ curve.

B. Antisymmetry/phase model

A general way to describe a parity-breaking bifurcation was proposed by Coullet, Goldstein, and Gunaratne [11]. The basic idea is to postulate a pitchfork bifurcation for the antisymmetry χ of the pattern (which can be understood in the k-$2k$ model as the phase shift between the k mode and the $2k$ harmonic), and to introduce a link between the phase ϕ and the antisymmetry χ. This leads to the following system of coupled equations:

$$\chi_t=\mu\chi-\alpha\chi^3, \qquad \phi_t=\omega\chi, \tag{6}$$

where all the parameters are real and μ is the control parameter of the PB state.

In a spatially extended system, these coupled equations with all the terms allowed by the symmetries [13] are given by

$$\chi_t=d\chi_{xx}+\varepsilon\phi_x\chi+\mu\chi-\alpha\chi^3+a_1\phi_{xx}+\gamma\chi\chi_x+b_1\phi_x\phi_{xx}, \qquad \phi_t=D\phi_{xx}+\omega\chi+a_2\chi_{xx}+c_2\chi\chi_x+d_2\phi_x\phi_{xx}. \tag{7}$$

Fauve, Douady, and Thual [12] and Riecke and Paap [27] showed that the term $\varepsilon\phi_x\chi$ makes the PB-state phase unstable just beyond the bifurcation where it should appear. However, it has been shown that inclusions of such a parity-breaking state may exist [28,18,26].

In our case, we want to study what happens before the parity-breaking bifurcation takes place. We will therefore study the following system where all the second-order and third-order terms are neglected:

$$\chi_t=\mu\chi+d\chi_{xx}+a_1\phi_{xx}, \qquad \phi_t=\omega\chi+D\phi_{xx}+a_2\chi_{xx}. \tag{8}$$

In this system, μ is negative and D and d represent the ''natural'' diffusion. Conversely, the a_1 term introduces the effect of phase inhomogeneities on the antisymmetry of the pattern, which is a fairly natural effect that would otherwise not be taken into account. The a_2 term will be considered to be weak against the $\omega\chi$ term.

This linear system leads to a dispersion relation for normal modes of the following form:

$$\phi=\phi_o\exp(st)\exp(iqx), \qquad \chi=\chi_o\exp(st)\exp(iqx). \tag{9}$$

Introducing these expressions in Eq. (8), one reaches an eigenvalue problem for which the discriminant is to the order q^2

$$\Delta(q)=\mu^2-2(d-D)\mu q^2-4a_1\omega q^2. \tag{10}$$

The eigenvalues s are written as

$$s=\frac{\mu-(d+D)q^2\pm\sqrt{\Delta(q)}}{2}. \tag{11}$$

In the limit $q\to 0$ this relation is written $s=\mu$ (damped mode) and

$$s=-\left(D-\frac{a_1\omega}{\mu}\right)q^2. \tag{12}$$

Equation (12) leads to a phase-diffusion equation:

$$\phi_t=D'\phi_{xx} \quad \text{with} \quad D'=D-\frac{a_1\omega}{\mu}. \tag{13}$$

It is therefore shown that if the term $a_1\omega$ is positive, the effective phase-diffusion coefficient D' actually diverges in the vicinity of any parity-breaking bifurcation as $\mu\to 0^-$. This behavior should be observed in various other experi-

mental systems. The measurement of the phase-diffusion constant could then be a tool of investigation to identify any parity-breaking bifurcation.

C. Consequence: Evanescent cavity modes

In a cavity of size L^*, the phase perturbation must be zero at the extremities of the interface, so the wave number q must be a multiple of π/L^* and cannot vanish. It is thus possible for $\Delta(q)$ to be negative for small μ if the term $a_1\omega$ is positive. If it is the case, s is complex and oscillatory states could exist in the cavity. For example if the term $a_1\omega$ is dominant in Eq. 10 $[\Delta(q)\approx -4a_1\omega q^2]$ the imaginary part of s corresponds to an oscillation of period

$$T=2\pi/(q\sqrt{a_1\omega}) \tag{14}$$

when the negative real part of s corresponds to a damping time

$$\tau=-2/[\mu-(d+D)q^2]. \tag{15}$$

This equation shows that the less-damped mode corresponds to the smallest mode of the cavity $(q^*=\pi/L^*)$. This mode will correspond to out-of-phase oscillation of ϕ and χ [Eq. (9)]. Similar oscillatory states, but not transient in character, were obtained theoretically in a parity-breaking bifurcation with an inhomogeneous system [29].

This analytical result on the existence of a transient oscillatory state is strongly analogous to the experimental results of II E. Indeed, we observe in Fig. 13 in-phase oscillations of the oil ribs. Thus, as time goes on, the interface alternately presents a pattern with asymmetric propagating air cells of homogeneous size and a pattern with symmetric air cells of inhomogeneous size. This behavior is exactly the one predicted by the previous analysis. Furthermore, the amplitude of the oscillation (Fig. 14) corresponds to the first resonant cavity mode $q^*=\pi/L^*$. Finally, Eq. (14) predicts that the oscillation period T is proportional to L^* if $q=q^*$. In Fig. 15 we indeed observe an increase of T that could be linear but not proportional to L^*.

IV. CONCLUSION

In this paper we addressed the wavelength-selection mechanism in a directional viscous fingering experiment. By the response of the interface to local periodic perturbations of the wave number, we observe a diffusive process of the phase perturbation and determine the corresponding diffusion constant D. From observation of the interface as well as measurements of D, we demonstrate first that, close to threshold, the wave-number range is controlled by the Eckhaus instability. For larger control-parameter values the wave number k is still limited by the Eckhaus instability in the large-k limit but not for low k. This low-k limit is characterized by a strong increase of D. This result and the shape of this low-k limit, when analyzed through a model of coupled equations for the k and $2k$ modes, suggest the proximity of a parity-breaking instability. We believe that this new wavelength-selection mechanism is general and should be encountered and demonstrated by the divergence of D in other systems presenting a bifurcation to asymmetric states.

Finally, long oscillatory transients of the pattern were occasionally observed and were interpreted in the same parity-breaking instability framework.

ACKNOWLEDGMENTS

We would like to especially thank Henry Thomé and Yves Couder for their help during the experiments and for fruitful discussions.

[1] M. C. Cross and P. C. Hohenberg, Rev. Mod. Phys. **65**, 851 (1993).

[2] G. Ahlers, D. S. Cannel, M. A. Domingez-Lerma, and R. Heinrichs, Physica D **23**, 202 (1986); H. Riecke and H.-G. Paap, Phys. Rev. A **33**, 547 (1986).

[3] *Hydrodynamic Instabilities and the Transition to Turbulence*, edited by H. L. Swinney and J. P. Gollub (Springer-Verlag, New York, 1985).

[4] J.-M. Flesselles, A. J. Simon, and A. J. Libchaber, Adv. Phys. **40**, 1 (1991); K. Kassner, C. Misbah, H. Müller-Krumbhaar, and A. Valance, Phys. Rev. E **49**, 5477 (1994).

[5] I. Mutabazi, J. J. Hegseth, C. D. Andereck, and J. E. Wesfreid, Phys. Rev. A **38**, 4752 (1988); I. Mutabazi and C. D. Andereck, Phys. Rev. Lett. **70**, 1429 (1993).

[6] M. Rabaud, S. Michalland, and Y. Couder, Phys. Rev. Lett. **64**, 184 (1990).

[7] L. Limat, P. Jenffer, B. Dagens, E. Touron, M. Fermigier, and J. E. Wesfreid, Physica D **61**, 166 (1992).

[8] W. Eckhaus, *Studies in Nonlinear Stability Theory* (Springer, New York, 1965); P. Manneville, *Dissipative Structures and Weak Turbulence* (Academic, San Diego, 1990); M. Lowe and J. P. Gollub, Phys. Rev. Lett. **55**, 2575 (1985); L. S. Tuckerman and D. Barkley, Physica D **46**, 57 (1990).

[9] F. H. Busse, Rev. Prog. Phys. **41**, 1929 (1978).

[10] M. C. Cross, P. G. Daniels, P. C. Hohenberg, and E. D. Siggia, J. Fluid Mech. **127**, 155 (1983); M. Dennin, D. S. Cannell, and G. Ahlers, Phys. Rev. E **49**, 462 (1994); S. S. Mao, J. R. de Bruyn, Z. A. Daya, and S. W. Morris, *ibid.* **54**, R1048 (1996).

[11] P. Coullet, R. E. Goldstein, and H. Gunaratne, Phys. Rev. Lett. **63**, 1954 (1989).

[12] S. Fauve, S. Douady, and O. Thual, J. Phys. II **1**, 311 (1991).

[13] B. Caroli, C. Caroli, and S. Fauve, J. Phys. I **2**, 281 (1992).

[14] L. Fourtune, W.-J. Rappel, and M. Rabaud, Phys. Rev. E **49**, R3576 (1994).

[15] L. Fourtune, thèse de l'Université Paris VI, 1994.

[16] S. F. Kistler and P. M. Schweizer, *Liquid Film Coating* (Chapmann and Hall, London, 1997).

[17] V. Hakim, M. Rabaud, H. Thomé, and Y. Couder, in *New Trends in Nonlinear Dynamics and Pattern Forming Phenomena*, edited by P. Coullet and P. Huerre (Plenum, New York, 1990), p. 327.

[18] H. Z. Cummins, L. Fourtune, and M. Rabaud, Phys. Rev. E **47**, 1727 (1993).

[19] M. Rabaud, Y. Couder, and S. Michalland, Eur. J. Mech. B/Fluids **10**, 253 (1991).
[20] J. E. Wesfreid and V. Croquette, Phys. Rev. Lett. **45**, 634 (1980).
[21] M. Wu and C. D. Andereck, Phys. Fluids A **4**, 2432 (1992).
[22] The transition between the two nucleation processes presented in Sec. II C was observed for $Ca/Ca^* \approx 1.32$. The present transition for the phase-diffusion behavior is observed around $Ca/Ca^* \approx 1.5$. Nevertheless these two values were obtained for two different sets of data, and the parallelism of the apparatus may have been modified meanwhile.
[23] U. Gerdts, J. Von Stamm, Th. Buzug, and G. Pfister, Phys. Rev. E **49**, 4019 (1994).
[24] M. R. E. Proctor and C. A. Jones, J. Fluid Mech. **188**, 301 (1988).
[25] W.-J. Rappel and H. Riecke, Phys. Rev. A **45**, 846 (1992).
[26] L. Pan and J. R. de Bruyn, Phys. Rev. Lett. **70**, 1791 (1993); Phys. Rev. E **49**, 2119 (1994).
[27] H. Riecke and H.-G. Paap, Phys. Rev. A **45**, 8605 (1992).
[28] R. J. Wiener and D. F. McAlister, Phys. Rev. Lett. **69**, 2915 (1992).
[29] E. Knobloch, J. Hettel, and G. Dangelmayr, Phys. Rev. Lett. **74**, 4839 (1995).